Journal of Atmospheric and Solar-Terrestrial Physics 112 (2014) 10–19

Contents lists available at ScienceDirect

Journal of Atmospheric and Solar-Terrestrial Physics

journal homepage: www.elsevier.com/locate/jastp

Study of local regularities in solar wind data and ground magnetograms

Virginia Klausner [a,c,*], Arian Ojeda González [a,1,2], Margarete Oliveira Domingues [b,3], Odim Mendes [a,4], Andres Reinaldo Rodriguez Papa [c,5,6]

[a] DGE/CEA/National Institute for Space Research – INPE, 12227-010 São José dos Campos, SP, Brazil
[b] LAC/CTE/National Institute for Space Research – INPE, 12227-010 São José dos Campos, SP, Brazil
[c] National Observatory – ON, 20921-400, RJ, Brazil

ARTICLE INFO

Article history:
Received 18 January 2013
Received in revised form
20 January 2014
Accepted 23 January 2014
Available online 19 February 2014

Keywords:
Wavelet analysis
Solar wind–magnetosphere interaction
Magnetogram data
Geomagnetic storm

ABSTRACT

Interplanetary coronal mass ejections (ICMEs) can reach the Earth's magnetosphere causing magnetic disturbances. For monitoring purposes, some satellites measure the interplanetary parameters which are related to energy transfer from solar wind into magnetosphere, while ground-based magnetometers measure the geomagnetic disturbance effects. Data from the ACE satellite and from some representative magnetometers were examined here via discrete wavelet transform (DWT). The increase in the amplitude of wavelet coefficients of solar wind parameters and geomagnetic field data is well-correlated with the arrival of the shock and sheath regions, and the sudden storm commencement and main phase, respectively. As an auxiliary tool to verify the disturbed magnetic fields identified by the DWT, we developed a new approach called effectiveness wavelet coefficient (EWC) methodology. The first interpretation of the results suggests that DWT and EWC can be effectively used to characterize the fluctuations on the solar wind parameters and their contributions to the geomagnetic field. Further, this kind of technique could be implemented in quasi real-time to facilitate the identification of the shock and the passage of the sheath region which sometimes can be followed by geoeffective magnetic clouds. Also, the technique shows to be very useful for the identification of time intervals in the dataset during geomagnetic storms which are associated to interplanetary parameters under very well defined conditions. It allows selecting ideal events for investigation of magnetic reconnection in order to highlight in a more precise manner the mechanisms existing in the electrodynamical coupling between the solar wind and the magnetosphere.

1. Introduction

An important kind of solar phenomenon is the coronal mass ejection (CME) because it can cause geomagnetic storms. This event can easily reach space regions close to 1 AU and it can be designated as an interplanetary coronal mass ejection (ICME). The term magnetic cloud (MC) is used to characterize an ICME having a specific configuration such as an enhanced magnetic field strength, a smooth rotation of the magnetic field vector and low proton temperature and plasma density (e.g., Burlaga et al., 1981; Klein and Burlaga, 1982; Gosling, 1990).

Near 1 AU, MCs have approximately 0.25 AU radial sizes with an average duration of 27 h, an average peak magnetic field strength of 18 nT, and an average solar wind speed of about 420 km/s (e.g., Klein and Burlaga, 1982; Goldstein, 1983; Lepping and Berdichevsky, 2000). Inside ICMEs, the measured plasma velocity has typically a linear variation along the spacecraft trajectory. However, a much higher velocity is present in the front of the MC than in its rear which indicates expansion (Démoulin and Dasso, 2009). Burlaga and Behannon (1982) found consistency between the expansion speed estimated from in situ observations and the increase of their typical size obtained from measurements with different spacecraft located between 2 and 4 AU. The MCs

* Corresponding author at: DGE/CEA/National Institute for Space Research – INPE, 12227-010 São José dos Campos, SP, Brazil.
Tel.: +55 12 32086819; fax: +55 12 32086810.
E-mail addresses: virginia@dge.inpe.br (V. Klausner), ojeda.gonzalez.a@gmail.com (A. Ojeda González), mo.domingues@lac.inpe.br (M. Oliveira Domingues), odim@dge.inpe.br (O. Mendes), papa@on.br (A. Reinaldo Rodriguez Papa).
[1] Department of Space Geophysics – IGA, Havana City, Cuba.
[2] Tel.: +55 12 32087854; fax: +55 12 32086810.
[3] Tel.: +55 12 32086542; fax: +55 12 32086375.
[4] Tel.: +55 12 32087854; fax: +55 12 32086810.
[5] State University of Rio de Janeiro – UERJ, 20550-900, RJ, Brazil.
[6] Tel.: +55 21 35049142; fax: +55 21 25807081.

http://dx.doi.org/10.1016/j.jastp.2014.01.013
1364-6826

closer than 1 AU to the Sun presented higher plasma densities than the surrounding solar wind. Thus, the density inside the flux tubes has a rapid decrease with the increasing distance from the Sun where the cloud undergoes a radial expansion.

When the MC is moving faster than the surrounding solar wind (SW), plasma and magnetic field accumulate, in principle, in front of it, forming a disturbed region called sheath region. The studies on the dynamics of those kinds of electrodynamic structures are among the current concerns of the space community (Bothmer and Schwenn, 1994; Ojeda et al., 2005, 2013; Chian and Muñoz, 2011). Many studies about the characteristics of MCs have been carried out over the last three decades (e.g., Klein and Burlaga, 1982; Lepping et al., 1990; Dasso et al., 2005; Ojeda et al., 2013). Many authors summarized the occurrence of interplanetary coronal mass ejection (ICME) in the near-Earth solar wind (Bothmer and Rust, 1997; Bothmer and Schwenn, 1998; Mulligan et al., 1998; Lynch et al., 2003; Wu et al., 2003; Huttunen et al., 2005; Nieves-Chinchilla et al., 2005; Cane and Richardson, 2003; Richardson and Cane, 2010). In this paper, we analyze solar plasma records concerning to the occurrence of ICMEs using an alternative wavelet technique algorithm developed by Mendes et al. (2005) and applied in Mendes da Costa et al. (2011) to study the geomagnetic storm behavior. Motivated by these earlier works, we deal with time variations of solar wind parameters due to solar events to verify their behaviors immediately before reaching the Earth, the "cause", and the "effect" of the solar wind–magnetosphere interaction, the geomagnetic storm, in ground magnetograms.

According to Farrugia et al. (1993), MCs can be used for the study of the solar wind energy input to the magnetosphere since the interplanetary magnetic field (IMF) components vary smoothly with time and retain the polarity for relatively long intervals. This is the main purpose of this work which provides an assessment to the electrodynamical coupling by investigating the level of regularity in "source" signal and "effect" signals. The efforts intend to verify the increase of wavelet coefficient amplitudes in signals associated to ICMEs propagation and to relate the effectiveness of this period of non-regularity with the development of geomagnetic storms. The proposed approach can be an auxiliary tool in the future for the investigation of solar wind energy transfers to the magnetosphere in periods of well-identified behavior. Thus, here, the discrete wavelet transform (DWT) has been applied to detect small (and nonlinear) transients in solar parameters and geomagnetic data. In order to develop this study, one year of data was investigated. The period of April 2001 which corresponds to the events during the solar maximum of the 23rd solar cycle was analyzed and presented as an example. Most of these magnetic storms in April 2001 were associated with MCs occurrence although shocks have also been observed.

The content of the paper is organized as follows. Section 2 is devoted to give a brief introduction on geomagnetic storms, showing an example of solar-interplanetary-magnetosphere coupling. Section 3 presents the data and the analyzed period, and the methodology implemented. Section 4 gives the results and a discussion on them. Finally, Section 5 brings the conclusion of this work.

2. Geomagnetic storm

The primary causes of geomagnetic storms are supposed to be strong dawn-to-dusk electric fields associated with the passage of southward directed interplanetary magnetic fields, B_s, passing the Earth for sufficiently long time intervals. The solar wind energy transfer mechanism is the magnetic reconnection between the IMF and the Earth's magnetic field (Dungey, 1961; Gonzalez et al., 1994). The most commonly used coupling function for the solar wind–magnetosphere interaction related to electric field is $E_y = VB_s$, see Gonzalez et al. (1994) for more details.

As a consequence, the level of magnetosphere activity varies widely. Geomagnetic activity is classified by intensity and usually described by the variation of indices to distinguish between a quiet and a disturbed day (occurrence of storms or substorms). The index mostly used in order to quantify the effects on low latitudes is the Dst index (Sugiura and Kamei, 1986), and more recently, Sym-H (Iyemori, 1990). Dst represents the variations of the H component due to changes of the ring current. The Sym-H is essentially a 1-min version of the traditional hourly Dst index. The main characteristic of the 1 min time resolution Sym-H index is that the effects of solar wind dynamic pressure variation are more clearly seen than in indices with lower time resolution (Wanliss and Showalter, 2006). Its calculation is based on magnetic data provided by eleven stations on low and medium latitudes. Each month only six stations are used for its calculation, some stations can be replaced by others depending on data conditions (Iyemori, 1990).

The principal defining property of a magnetic storm is the enhancement of the ring current due to the increase of the trapped magnetospheric particle population. These particles present a drift due to magnetic field curvature and gradient which leads the ions to move from midnight to dusk and electrons from midnight toward dawn surrounding the Earth close to the dip equator (Gonzalez et al., 1994).

The geomagnetic storms consist of four phases: sudden commencement, initial phase, main phase and recovery phase (Gonzalez et al., 1994). The characteristic signature of a magnetic storm is a depression in the horizontal component of the Earth's magnetic field (H) which is used to calculate the Dst index. In general, geomagnetic storms begin with a sudden impulse due to the arrival of the interplanetary shock structure (Sudden Storm Commencement – SSC) what generally coincides with the increased ram pressure and, consequently, an increase of the Dst values (initial phase) followed by a "negative excursion" in the Dst index which indicates sustained southward interplanetary fields (main phase) and the return to normal conditions (recovery phase) as discussed in Gonzalez et al. (1994).

3. Dataset and analysis methodology

In this section, we present the ACE satellite data used to characterize the variations of solar parameters due to ICMEs propagation. We will also present the data used to analyze the effects of the magnetospheric activity identified on the ground. Our study consists in verifying the magnetic events that occurred in April 2001. These solar events occurred during the solar maximum of the 23th solar cycle. The method used here is based on the Discrete Wavelet Transform (DWT) to verify the increase of wavelet coefficient amplitudes in the signals associated to the ICMEs propagation and to relate the effectiveness of this period of non-regularity to the development of geomagnetic storms.

3.1. ACE satellite data

In this paper, the effects of the solar activity upon the Earth and the space close to it were studied using ACE satellite data and the Sym-H index. Both of these datasets are available at the NOAA web site (SPIDR, 2008). The data for ground behavior analysis will be presented in the next section.

Our interest is to characterize the variations on the solar parameters related to the ICMEs propagation. For that reason, we selected the IMF components (Bx, By, Bz in GSE coordinate),

plasma density (N) and velocity (Vx component). We also use the Sym-H index to verify the global magnetic field reductions during storms. All datasets used in our analysis have 1 min resolution. Although one year of data was investigated, a short period was chosen to illustrate the application here developed. In April 2001, several solar disturbances happened which were detected by ACE instruments. Some ICMEs that caused geomagnetic disturbances in this period were previous studied by Wu et al. (2003), Huttunen et al. (2005), and Richardson and Cane (2010).

Table 1 is a slightly modified table from the work of Richardson and Cane (2010) and it is arranged as follows: column 1 gives the studied events defined by the letters from a to h. Column 2 gives the time of passage of an interplanetary shock at ACE and Column 3 gives the arrival of the ICME-driven shock at Earth. In this case, the time given is typically that of the geomagnetic storm sudden commencement (SSC), frequently accompanied by a shock reaching the Earth's magnetosphere since this provides a spacecraft-independent arrival time, which is also appropriate for comparison with phenomena at Earth. Column 4 gives the disturbance time to the start time of the ICME; if no upstream disturbance is evident, then the disturbance time listed corresponds to the start time of the ICME, otherwise they are different. Column 5 shows the ICME end time. Columns 6 and 7 give the offsets (in hours) of the magnetic cloud leading and trailing boundaries relative to the ICME boundaries ($t_{mc}-t_{ICME}$), based primarily on the WIND magnetic cloud list. Additional events identified by Huttunen et al. (2005) are also included and identified by a * notation. A "2" in Column 8 indicates that the ICME includes a MC reported on the WIND magnetic cloud list or in Huttunen et al. (2005). A "1" indicates that there is evidence of a rotation in the magnetic field direction, but overall, the magnetic field characteristics do not meet those of a magnetic cloud. Events with no magnetic cloud-like magnetic field features are indicated by "0". The minimum geomagnetic Dst value is given in Column 9.

3.2. Ground magnetic data

The magnetic stations considered in the analysis are Honolulu (HON), San Juan (SJG), Vassouras (VSS), Hermanus (HER) and Kakioka (KAK). We examine how the effects within the magnetic storms in April 2001 look like. They are consequence mainly of the global space and time configuration of the ring current at low-latitudes and the additional variations of the H-component related to the effect of equatorwards penetration of electric fields from the field-aligned current (Wu et al., 2004). The selected magnetic stations are used to calculate the Dst index, except by VSS.

Another point of interest is the correlation of the responses of chosen stations due to the development of geomagnetic storms. The geographic and geomagnetic localization of stations are shown in Table 2.

3.3. Discrete orthogonal wavelet transform (DWT)

The discrete orthogonal wavelet transform is a linear multiscale transform that can deal with non-stationary signals and, specially here, helps on the study of its local regularity. Namely, the discrete wavelet coefficients are given by the square integrable functional space L^2 inner-product

$$d_k^j = \int f(t)\psi(2^j t-k)\,dt, \quad j,k\in\mathbb{Z}, \tag{1}$$

where the function ψ is the analyzing wavelet function, and j and k are the scale and position parameters, respectively. In this work, we choose the Daubechies order-2 analyzing wavelet. A good generic review on that transform can be found in Hubbard (1990) and there are many good textbooks on this subject, for instance Daubechies (1990) and Mallat (1997).

The multiscale aspects of this transform help us to study specific phenomena scales associate to central frequencies (also called pseudo-frequency) and how they change as the time evolves. Therefore, this wavelet orthogonal transform can be used to detect disturbances in specific scales using its propriety of local regularity detection based on the decay of the square wavelet coefficient amplitudes. In the first part of Appendix A, it is described briefly the multiresolution tool, the so-called Mallat pyramidal algorithm, and the theorem that defines the local regularity. Related to the last feature, the key aspect is that the amplitude of the wavelet coefficients can be associated to the local polynomial approximation error. The larger those coefficients are, more disturbed the signal is. By choosing an analyzing wavelet function, we define which local polynomial approximation we have, and so the local error obtained in this approximation is stored in the wavelet coefficients (Mendes et al., 2005). Those errors could also detect the local regularity of high order derivatives of the analyzing function. Normally, that feature cannot be seen by visual inspection. This property is presented in the last part of Appendix A.

During the visual inspection of a signal, someone can easily lost some disturbances, specially in large datasets, and/or also it could

Table 2
INTERMAGNET network of geomagnetic stations used in this study.

Station	IAGA code	Geographic coord.		Geomagnetic coord.	
		Lat. (°)	Long. (°)	Lat. (°)	Long. (°)
Honolulu (United States)	HON	21.32	−158.00	21.59	−89.70
San Juan (Puerto Rico)	SJG	18.12	−66.15	27.93	6.53
Vassouras (Brazil)	VSS	−22.40	−43.65	−13.43	27.06
Hermanus (South Africa)	HER	−34.41	19.23	−33.89	84.68
Kakioka (Japan)	KAK	36.23	140.18	27.46	−150.78

Source: http://wdc.kugi.kyoto-u.ac.jp/igrf/gggm/index.html (2010).

Table 1
Near-Earth ICMEs in 2001, April.

Column 1 Event	2 Shock (ACE) mon/day UT	3 Disturbance mon/day UT	4 ICME Start mon/day UT	5 ICME End mon/day UT	6 Start MC	7 End MC	8 MC?	9 Dst (nT)
2001								
a	04/04 1422	04/04 1455	04/04 1800	04/05 1200	0	−4	2	−50
b	04/08 1032	04/08 1101	04/08 1400	04/09 0400	...	...	0	−59
c	04/11 1314	04/11 1343	04/11 2200	04/13 0700	+10	−13	2*	−271
d	04/13 0706	04/13 0734	04/13 0900	04/14 1200	...	...	0	−77
e	...	04/15 1700	04/15 1700	04/16 0100	...	...	0	−36
f	04/18 0015	04/18 0046	04/18 1200	04/20 1100	...	...	0	−114
g	04/21 1508	04/21 1601	04/21 2300	04/23 0300	0	...	2*	−102
h	04/28 0431	04/28 0501	04/28 1400	05/01 0200	+12	...	2*	−47

Source: adapted from Richardson and Cane (2010).

be lead to different interpretations and classifications of the same signal, specially when the disturbs are associated to a higher order derivatives. This square amplitude of the wavelet coefficient representation associated to the chosen scale is an efficient and objective way to deal with it. Therefore, this tool provides a quantitative measure by squaring the amplitude of the wavelet coefficients of these local approximation errors.

This kind of methodology to identify disturbances is popular in wavelet adaptive numerical modeling to automatically identify structures in the solution and refine the grids only in these regions, see for instance Müller (2003) and Domingues et al. (2009, 2011, 2008). As well as, this technique can be applied in different areas with wider detection purposes, a proper choice of the analyzing wavelet function, the scale, and the kind of disturbance associated to the wavelet coefficient amplitudes are very important.

Moreover, as this is an orthogonal transform the square amplitudes represent also the local signal energy in L^2 sense, therefore we can also analyze it as a multiscale energy contribution in the total signal energy. This energy conservation follows the same idea as the so-called Paserval theorem in Fourier analysis.

In this paper, we only study the discrete scales $j=1$, 2, and 3 which are associate to the central frequencies of 3, 6, and 12 min, respectively. These central frequencies values are obtained due to our analyzing wavelet choice and to the data sample rate of 1 min time resolution, more details in Abry (1997), Mendes et al. (2005) and Appendix A. From the physical point of view, on the ACE dataset, these pseudo-periods may be related to turbulent magnetic fields due to the passage of the sheath region and, on the ground magnetogram data, these pseudo-periods may be related to Pci 5 pulsations.

In order to enhance the visualizations of the integrate local energy contributions in the wavelet coefficients, we construct the daily index EWC - Effectiveness Wavelet Coefficients, with the following expression

$$EWC=\frac{1}{7}\left(4\sum_{k}^{N}|d_k^{j=1}|^2+2\sum_{k}^{N}|d_k^{j=2}|^2+\sum_{k}^{N}|d_k^{j=3}|^2\right), \quad (2)$$

where the k-summations are for one day, $N=1440$, considering our original signals with 1 min resolution. The EWC is weighted according to the scale decomposition levels to better highlight the small scale disturbances. The daily interval was chosen to allow classifying the behavior in a complete day. The parcels are weighted to enhance irregularities in shorter periods.

The empirical choice of the weighted values 4, 2 and 1 is based on the DWT computation where the signal is reduced by half length in each level of decomposition. Also, we decided to use one day resolution because the EWC is only an estimator of the parameter disturbances. This was done in order to facilitate the visualization of the three levels of the wavelet decomposition which have a resolution of 1 min. In other words, the EWC is just the integration of the wavelet coefficients during 24 h (one day), however any other kind of resolution can be applied.

4. Results and discussion

In this section, we first analyze the solar wind parameters to verify ICME behaviors before reaching the Earth, the "cause" of the geomagnetic storms. Second, we verify the "effect" of the solar wind–magnetosphere interaction, the geomagnetic storm, in ground magnetograms. Following, we examine the correlations between the "cause" and the "effect".

4.1. ACE

Fig. 1 is divided in to four panels. At top left, it shows the behavior of the solar wind parameters (IMF components (Bx, By, Bz in GSE coordinate), plasma density and velocity (Vx)) for April 2001. At top right, bottom left and bottom right, the panels show the behavior of the square wavelet coefficients for these solar wind parameters at the three first levels $j=1$, 2 and 3, denoted by d^1, d^2, d^3, respectively. The horizontal axis of each panel has one day time resolution. In all panels, we highlighted the events listed in Table 1. We used continuous lines to indicate the start and the end of each ICME event (from "a" to "h"). We also used dashed lines in red to indicate the shock arrival time at ACE, in green, for the MCs arrival time and in light blue, for MCs stop time.

As mentioned in the methodology (see Section 3.3) the wavelet coefficients are able to identify the variations of the ACE parameters due to solar wind events with different properties and degrees of disturbance. The MCs events shown in Table 1 were all identified by the decrease of wavelets coefficients at the three decomposition levels that followed the increase of wavelets coefficients due to the shock and the turbulent fields of the sheath region.

In Fig. 1, the MC event "a" was not identified by Huttunen et al. (2005), however this MC was published by Wu et al. (2003) /WIND list (with quality: 1=excellent), and also reported in the work of Nieves-Chinchilla et al. (2005). It is a bipolar cloud with a flux rope type NWS and the observed angular variation of the magnetic field is left-handed. Some features related to the ICME classified as MC in April 04–05 were reported by Richardson and Cane (2010): $V_{ICME}=650$ km/s, V_{ICME} is the mean SW speed in the ICME; $V_{max}=780$ km/s, the maximum SW speed in the post disturbance region; $B=9$ nT, the mean field strength; and $V_T=1020$ km/s, the transit speed. The Dst index shows one geomagnetic storm, with $Dst_{min}=-50$ nT caused by this MC. It is possible to identify, in the MC event "a", an increase in the amplitude of the wavelet coefficients at the three levels of decomposition due to the shock and to the passage of the sheath region in Fig. 1.

The MC event of WNE-type (event "c") was identified by the simultaneous decrease in the amplitude of the wavelet coefficients at the three decomposition levels after their increase provoked by the shock and the passage of the sheath region. The Dst index shows one geomagnetic storms with $Dst_{min}=-271$ nT caused by the plasma sheath (Huttunen et al., 2005). A great number of wavelet coefficients presenting an increase of amplitude was found between the shock and the MC starting time at all three levels of decomposition. These wavelet structures are associated to the sheath, region of solar wind bounded by the shock front and the ICME leading edge (Owens et al., 2005). Also, the Bz-component has the same sign during the MC propagation and it has the axis highly inclined to the ecliptic (Unipolar MCs).

The MC event with WSE flux rope type (event "g") was also detected by the decrease of wavelet coefficient amplitude after their increase due to the shock and sheath region. This event caused medium degree of disturbance of Dst index according to NOAA classification ($Dst_{min}=-103$ nT). The plasma density presented wavelet structures during the shock and the sheath region at all three levels of decomposition.

This could be a consequence of the low values of plasma density associated with this particular event in the solar wind. The shock and the passage of the sheath region preceding the MC event of SEN-type (event "h") were also identified by an increase in wavelet coefficient amplitude. Their wavelet structures were very similar to the second MC (event "c"). However, these events were considered of low degree of disturbance by Dst index ($Dst_{min}=-33$ nT).

Apart from the MCs events, the wavelet coefficients also presented an increase of amplitude during other periods of time.

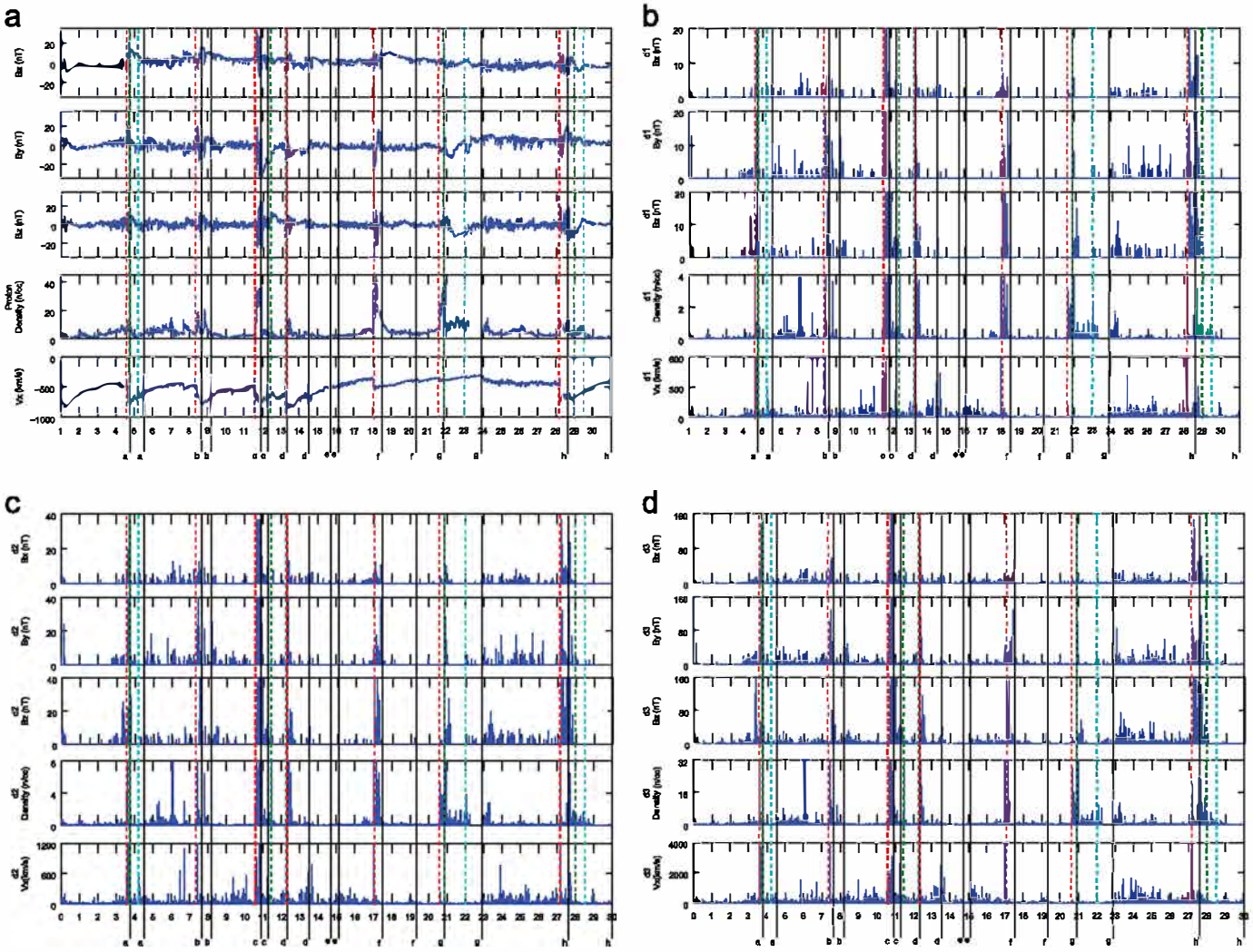

Fig. 1. ACE: (a) Magnetic field components (X, Y and Z), plasma density, velocity (X-component); and (b–d) the wavelet coefficients $(d^j)^2$ for $j=1$, 2, 3, respectively. The horizontal axis of each panel has one day time resolution. (a) ACE data, (b) $(d^j)^2$ for $j=1$, (c) $(d^j)^2$ for $j=2$ and (d) $(d^j)^2$ for $j=3$. (For interpretation of the references to color in this figure caption, the reader is referred to the web version of this article.)

This fact could be associated to the ICMEs occurrence and, consequently, to their driven shock as it propagates towards the ACE satellite.

Altogether, the wavelet structures were increased during the shock and the sheath region at all three levels of decomposition for all the MC events mentioned above, and also, for all ICME shock events.

Fig. 2 shows EWCs in April 2001 for the ACE datasets. On the vertical axis, each panel presents the weighted geometric mean of the square wavelet coefficients per hour, in other words, the EWCs, and, on the horizontal axis, the time resolution of a day. Also, we highlighted the events listed in Table 1 in the same way we did in Fig. 1. On the analysis of the IMF components, the wavelet coefficients present higher amplitudes during the shock and the sheath region of the events "c" and "h". However, the event "g" was better detected by EWCs of plasma density than by the IMF components, during its shock and sheath region. There was also an increase of EWCs amplitude of all solar parameters during the event "h" shock and sheath region.

It can be noted an increase of EWCs on the IMF components that correspond to the shock and sheath region propagation on the events "a", "b", "c", "f", "g" and "h". On events "d" and "e", the EWCs also presented a slight increase in amplitude. As noticed in Fig. 2, the larger EWC amplitudes of these solar wind parameters occur during the shock and sheath region.

4.2. Ground magnetic data analysis

Fig. 3 shows four panels presenting (a) the ground magnetograms and (b–d) the first three decomposition levels.

Each panel displays, from top to bottom, the data or results for the magnetic stations of Honolulu (HON), San Juan (SJG), Vassouras (VSS), Hermanus (HER) and Kakioka (KAK). The horizontal axis of each panel has time resolution of one day.

In the four panels, we highlight the events listed in Table 1. We used continuous lines to indicate the start and the end of each ICME event (from "a" to "h"). We also used dashed lines in light green to indicate the geomagnetic storm sudden commencement, and in orange, the main phase.

In Fig. 3(a), we observe a magnetic signature of few geomagnetic storms with different magnitudes. The major geomagnetic storms of April 2001 were defined as: event "a" started in April 4, 2001 with $Dst_{min} = -50$ nT at 08:00 UT in April 5, event "b" started in April 8, 2001 with $Dst_{min} = -63$ nT at 07:00 UT in April 9, event "c" – a very-intense magnetic storm with $Dst_{min} = -271$ nT at 24:00 UT in April 11, 2001, event "f" – an intense magnetic storm in April 18, 2001 with $Dst_{min} = -114$ nT at 08:00 UT, event "g" – other intense storm started in April 21, 2001 with $Dst_{min} = -102$ nT, and event "h" occurred in April 28, 2001 with $Dst_{min} = -47$ nT.

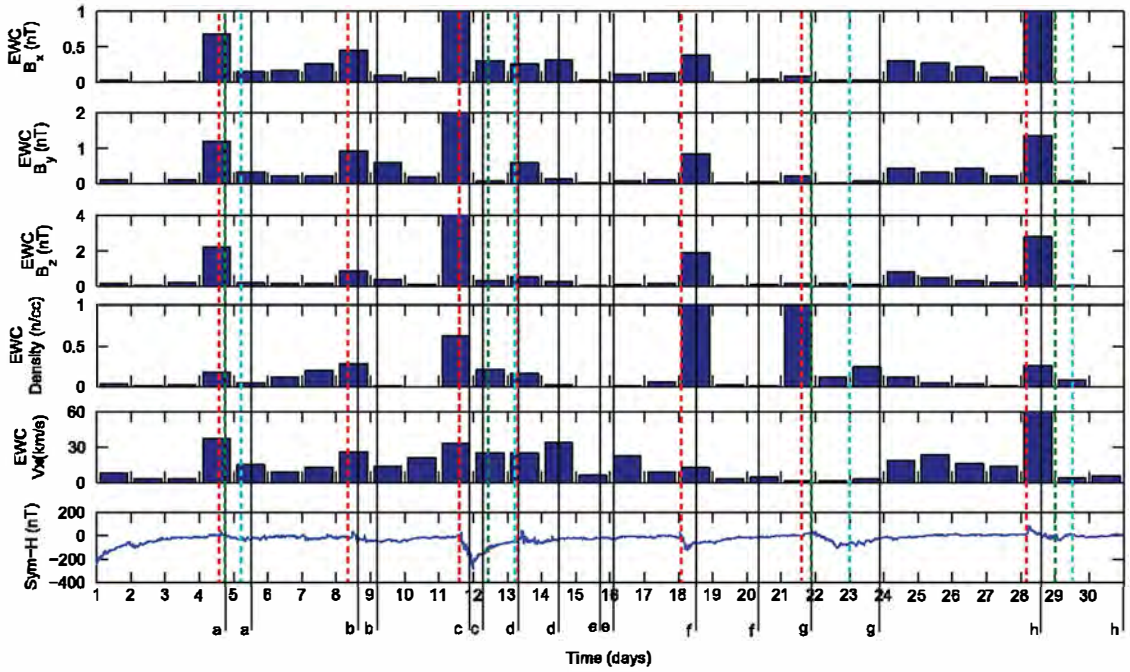

Fig. 2. The effectiveness wavelet coefficients in April 2001 for the ACE dataset which are the integration of the wavelet coefficients at the three levels of decomposition during 24 h (one day). The continuous lines indicate the start and the end of each ICME event ("a" to "h"), the dashed lines in red indicate the shock arrival time at ACE, in green, indicate the MCs arrival time, and in light blue, indicate the MCs stop time. The Sym-H index is used only to identify the disturbances on the geomagnetic field. (For interpretation of the references to color in this figure caption, the reader is referred to the web version of this article.)

We observe an increase in coefficient amplitudes during the SSC, and also during the main phase of geomagnetic storms. It is possible to note that the wavelet coefficients presented an increase by the arrival time of the ICMEs when it reaches Earth's magnetosphere. All the magnetic stations showed similar patterns of magnetic behavior response to the storms with just a few singularities in the three levels of wavelet decomposition. As Mendes et al. (2005) suggested, this behavior may be related to differences in the magnetic coordinates, type of magnetometer used, local time, ground conductivity and Sq currents effects.

In Fig. 4, where the EWCs for the month April 2001 are presented, it is also possible to notice that the higher EWC amplitudes are related to the SSC, and to the main phase of geomagnetic storm.

4.3. ACE and ground data correlation analysis

In the ACE parameter analysis, there was an increase of wavelet coefficient amplitudes and EWCs of the IMF components during shock and sheath region. They can start a geomagnetic storm because during the passage of a sheath, the shock compression, turbulence, magnetic field draping or shock heliospheric current sheet may lead to southward magnetic fields (Badruddin, 2002). As Gonzalez and Tsurutani (1987) discussed, a geomagnetic storm occurs when the interplanetary magnetic field turns southward and remains southward for a prolonged period of time.

In April 2001, the ACE satellite detected solar wind events about 30–80 min before they arrived to the Earth's magnetosphere. The delay values can be obtained from Space Physics Interactive Data Resource (SPIDR, 2008) site.

The SSC occurs due to the sudden impulse received in the arrival of the interplanetary shock structure which generally coincides with the increased ram pressure (initial phase) followed by the decrease of geomagnetic field (main phase) which indicates sustained southward interplanetary fields in the sheath region or/and during the MC propagation (Gonzalez et al., 1994). It was possible to note a simultaneous increase of EWC values in Figs. 2 and 4, respectively at the shock and SSC regions; and at the sheath and main phase regions. The EWC hourly values disguises the arrival delay of the shock and sheath region at the Earth's magnetospause. On the analysis of ground magnetograms, the highest coefficient amplitude was coincident in time, showing that the whole magnetosphere is globally affected, at least in the time resolution considered as discussed in Mendes et al. (2005). The amplitude of the EWCs is related to geoeffectiveness of solar events. It is also worth to mention that the small amplitudes of the wavelet coefficients mean that the energy transfer process is smooth; while the large amplitudes indicated that there were impulsive energy injections superposed to the smooth background process.

This paper brings a new alternative way to visualize the wavelet coefficients based on the integration of local energy contributions of these coefficients in each scale, the Effectiveness Wavelet Coefficients (EWC). The EWC facilitates the analysis of wavelet coefficients because it presents a simple representation instead of the traditional discrete wavelet transform (DWT) that has many levels (in our case, we choose three levels of the wavelet decomposition).

The wavelet coefficients algorithm was developed by Mendes et al. (2005) and used in the following work of Mendes da Costa et al. (2011) to study geomagnetic storm behaviors. On their work, this technique proved to be very efficient to detect local irregularities on ground magnetograms due to geomagnetic storms. Here, we advance the use of wavelet coefficients to study, as well, the local irregularities of interplanetary parameters (Bx, By, Bz, Vx and Density). By applying DWT on the interplanetary parameters, we were able to analyze the fluctuations in each parameter, and after, we compared them with the fluctuations on the ground magnetograms. The DWT, and consequently the EWC, detected the shock and sheath region passage, "cause", and on the ground, the SSC and the main phase of geomagnetic storm, "effect". One as consequence of the other. For these reasons and with further analysis, the DWT and EWC tools could be implemented in quasi-real-time analysis to facilitate the identification of ICMEs and also their corresponding geoeffectivity effects.

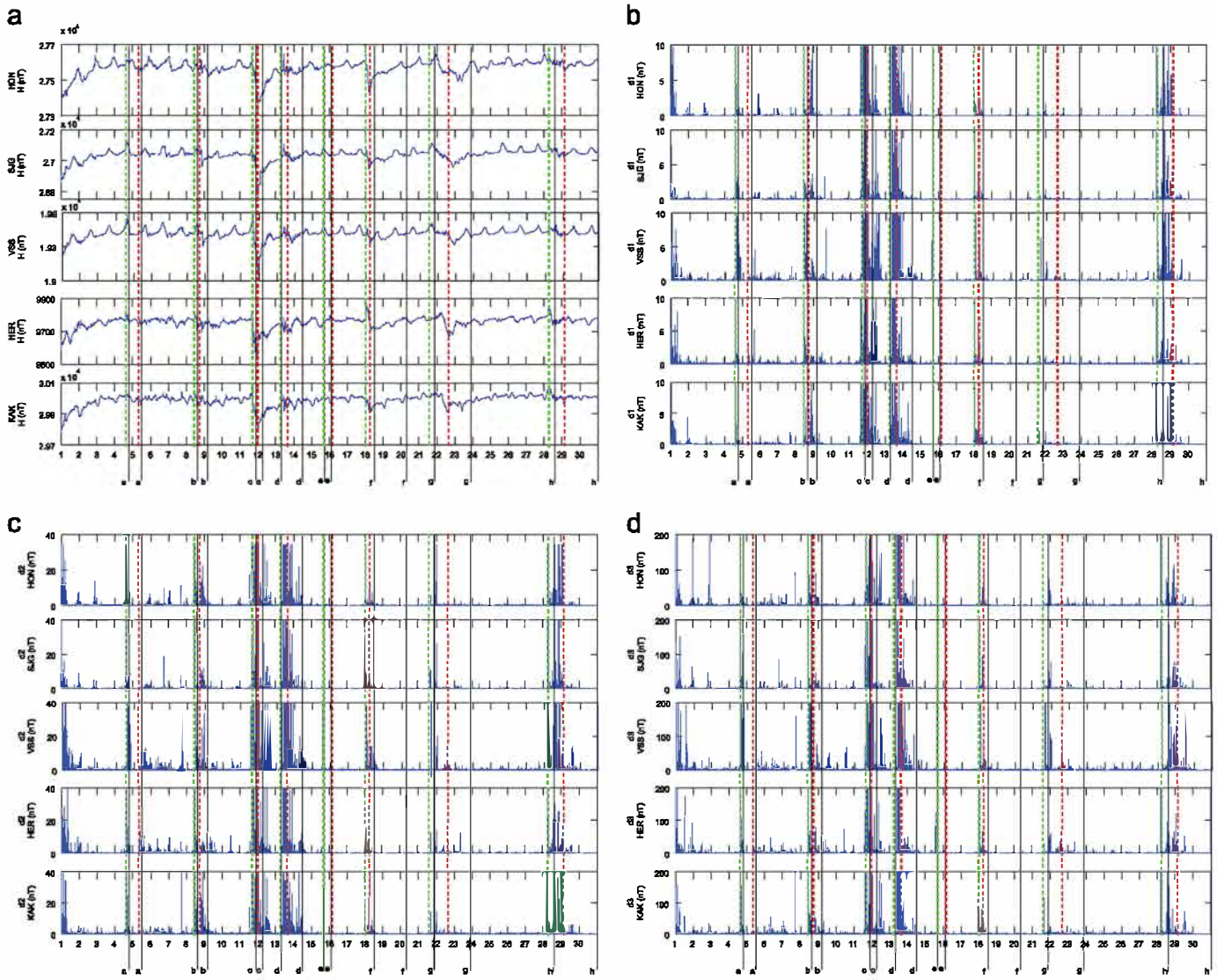

Fig. 3. Ground: (a) magnetograms and Sym-H index; and (b–d) the wavelet coefficients $(d^j)^2$ for $j=1, 2, 3$, respectively. The horizontal axis of each panel has one day time resolution. (a) Ground data, (b) $(d^j)^2$ for $j=1$, (c) $(d^j)^2$ for $j=2$ and (d) $(d^j)^2$ for $j=3$. (For interpretation of the references to color in this figure caption, the reader is referred to the web version of this article.)

5. Conclusions

In this work, we investigate the magnetic disturbances that occurred in April 2001 using a new methodology based on the amplitude of the discrete wavelet coefficients applied to solar wind and magnetogram datasets. We explored the solar parameters detected by the ACE satellite and the H-component of magnetic field measured by ground magnetometers at HON, SJG, VSS, HER and KAK.

In response to the disturbances, the results show that the increase of wavelet coefficient amplitudes associated with solar wind parameters appears to occur at the same time with the passage of shock and sheath regions. In the ground magnetograms analysis, the increase of wavelet coefficient amplitude is associated with the sudden storm commencement (SSC) and the main phase of geomagnetic storm. The increase of wavelet coefficient amplitudes due to the passage of shock and sheath regions always occurs a few minutes earlier than the SSC and main phase and, one is a consequence of the other.

The EWC approach aims to facilitate the analysis and characterization of interplanetary phenomena and their interaction with the Earth's magnetosphere requiring minor effort. The shock and the passage of sheath region, and also, the magnetic activity measured on ground are characterized by the increase of EWC, both easily detected even by untrained eyes. The advantage of EWC is that it has a simple integrated representation while the previous studies employed three decomposition levels. However, this tool does not reduce the analysis effort to zero, it is always assisted by the three levels of wavelet decomposition which present lower resolution (in this case, 1 min) and a higher degree of detail.

Our methodology could be used in an automatic way to characterize the solar wind and ground magnetic disturbances. It could be important to improve the knowledge of the peculiarities and the effects produced by solar events on the Earth's magnetosphere and further it could be implemented to quasi-real-time analysis to facilitate the identification of ICMEs, since it was able to identify the shock and the passage of the sheath region, which sometimes could be followed by geoeffective MCs. It could predict a potential geomagnetic storm development.

Similar results are obtained considering larger datasets, for instance one year of data. As a general result, the technique helps to identify data intervals with high regularity regime from intervals with very low regularity. Although the presence of low

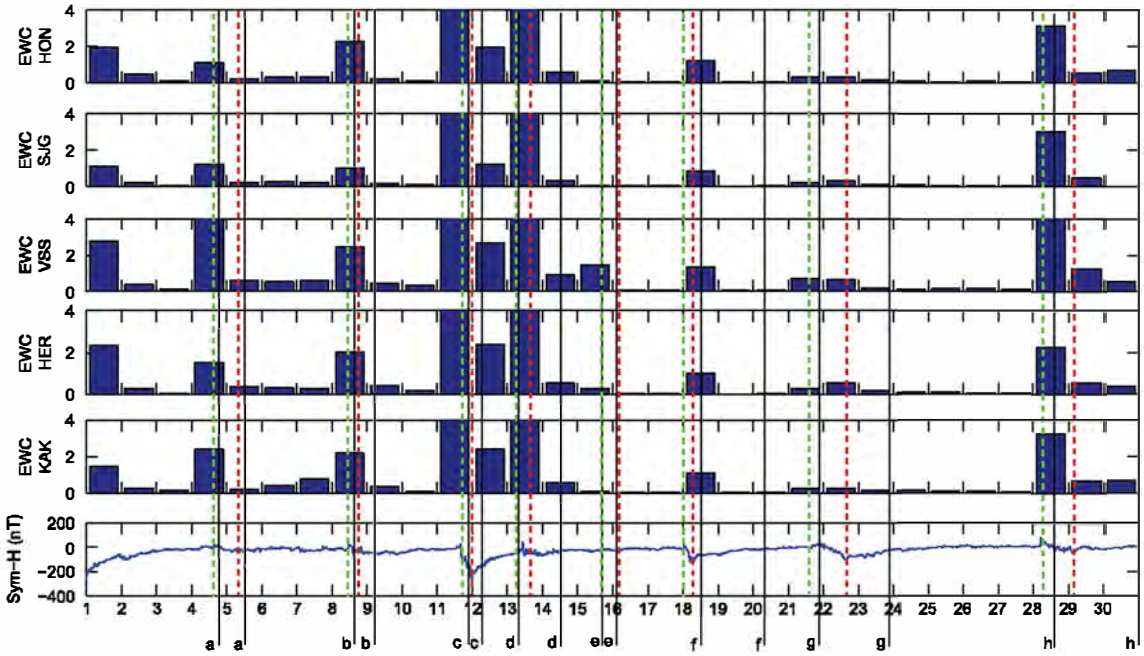

Fig. 4. The effectiveness wavelet coefficients in April 2001 for the ground magnetograms which are the integration of the wavelet coefficients at the three levels of decomposition during 24 h (one day). The continuous lines indicate the start and the end of each ICME event (from "a" to "h"), the dashed lines in light green indicate the geomagnetic storm sudden commencement, and the dashed lines in orange indicate the geomagnetic main phase. The Sym-H index is used only to identify the disturbances on the geomagnetic field. (For interpretation of the references to color in this figure caption, the reader is referred to the web version of this article.)

regularity in the geomagnetic records on the ground for middle-low latitude observatories corresponds to solar wind disturbance acting upon the Earth's magnetosphere, reciprocity is not always valid. Other kinds of phenomena can be occurring upon the magnetosphere-system, which motivate other new studies. Nevertheless, the technique shows to be very useful for the identification of time intervals in the dataset during geomagnetic storms that correspond to interplanetary parameters under behaviors very well defined. It allows selecting ideal events for the investigation of magnetic reconnection in order to highlight in a more precise manner the mechanisms existing in the electrodynamical coupling between the solar wind and the magnetosphere.

Acknowledgments

This work was supported by CAPES (Grants 465/2008, 86/2010-29, 0880/08-6, 86/2010-29, 551006/2011-0, and 17002/2012-8), CNPq (Grants ISOS95/2013-1, 141549/2010-6, 309017/2007-6, 486165/2006-0, 308680/2007-3, 478707/2003, 477819/2003-6, 382465/01-6), FAPESP (Grants 2011/20588-7, 2007/07723-7, 304856/2012-6, and 303043/2009-1). The authors would like to thank the NOAA and the INTERMAGNET programme for the datasets used in this work and V. Menconi and M. Correa for their helpful assistance. The authors are indebted to the anonymous referees whose comments and suggestions contributed to improve this work.

Appendix A. Wavelet for local regularity analysis

Multiresolution analysis consists of a multiscale approximation designed method. Under it, a functional squared integral space $\mathbb{L}^2$ is represented by a sequence of nested subspaces $\cdots V^0 \supset V^1 \supset V^2 \cdots$ that satisfies certain self-similarity relations in time and scale, as well as completeness and regularity relations. This analysis was introduced in Mallat (1997).

Self-similarity in time demands that each subspace is invariant under shifts, in this case, by integer multiples of 2^k, and self-similarity in scale, j, demands that all subspaces are time-scaled versions of each other. Regularity demands that the subspace V^0 be generated as the linear hull of the integer shifts of a finite number of generating functions $\phi(t) := \sum_k h(k)\phi(2t-k)$ that form a Riesz base of this subspace, where h is the low-pass filter. In most cases those functions are piecewise continuous with compact support (Daubechies, 1990). Completeness demands that those nested subspaces fill the whole space $\mathbb{L}^2$, and their intersection should contain only the zero element. Consequently, we have the complementary space W^j with a Riesz basis $\psi(t) := \sum_k (-1)^{(1-k)} h(1-k)\phi(2t-k)$, called wavelet function, such that $V^{j-1} = V^j + W^j$. The W^j subspaces fill the whole space $\mathbb{L}^2$.

This tool helps in the construction of analyzing wavelet function based on this scale functions, with desired mathematical proprieties, such as compact support, desired number of vanishing moments, and local polynomial reproduction of a determined order of approximation. For instance, a wavelet function has p vanishing moments if and only if its scaling function can be generated by polynomials up to degree $p-1$. This implies that the wavelet coefficients are zero for polynomials of degree at most $p-1$, that is, the scaling function alone can be used to represent such functions locally. More vanishing moments mean that more complex functions can be represented with a sparser set of wavelet coefficients. The wavelet coefficient can be considered as a local approximation error. As a result of such construction the decay of the wavelet coefficients can be used as local indicators of regularity of the analyzed signal as presented in the following theorem.

Theorem. *Considering $p+1$ the number of vanishing moments of $\psi(t)$. If $f(t)$ is an uniformly Lipchitiz function and $f^{(s)}$ is your derivative function over the whole support of $\psi(2^j t-k)$, where $0 \le s \le p+1$, then the wavelet coefficients d_k^j obtained in the discrete wavelet transform are $d_k^j = \int f(t)\psi(2^j-k)\,dt$, satisfy $|d_k^j| \ge c2^{-j(s+1/2)}\|f^{(s)}\|$ where c is a constant which depends of ψ and $\|f^{(s)}\|$ is the norm of $f^{(s)}$ in ψ_k^j.*

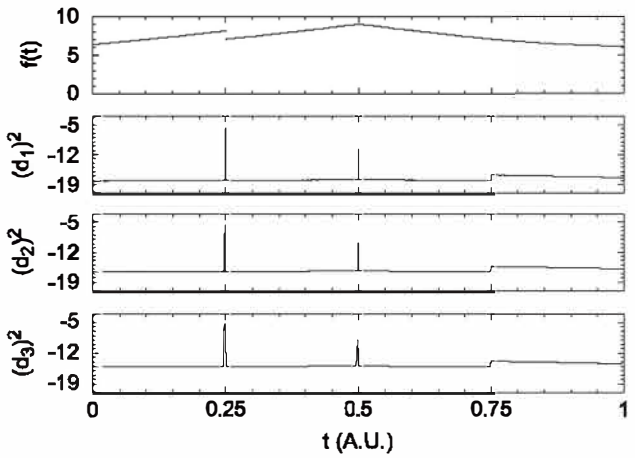

Fig. A1. At top, the signal $f(t)$ and, below ,the logarithm of the square of the first three decomposition levels of wavelet coefficients ($d_1^2(t)$, $d_2^2(t)$ and $d_3^2(t)$).

Moreover based on that tool, Mallat designed a fast discrete wavelet transform constructed with filter bank pyramidal algorithms.

In this work, we use the Daubechies wavelet of order 2, that approximate locally linear functions, i.e., $p=1$. For this wavelet the non-zero values of h filter are irrational numbers, namely, $h \cong$ [0.48296291314453414337487 16, 0.83651630373780790557529 4, 0.22414386804201338102597 3, −0.12940952255126038117444 94], for $k=1$–4 .

This part illustrates the skill of wavelet technique (the Daubechies orthogonal wavelet of order 2) to identify regions of regularity in signals as used in this work. If the signal can be approximated locally by linear functions, then the wavelet coefficients are zero in those regions. Moreover, the amplitude of the wavelet coefficients can be used in the detection of the local discontinuities both in signal and in its high order derivatives. As smaller is the amplitude of the wavelet coefficients, as smoother is the signal.

In order to help understanding, someone can consider a synthetic signal $f(t)$, where t is the time in this example, given as follows:

$$f(t)=\begin{cases} 8.1\ e^{1/4}\ e^{-|t-(1/2)|} & \text{if } t\le\frac{1}{4},\\ 9\ e^{-|t-(1/2)|} & \text{if } \frac{1}{4}\le t\le\frac{3}{4},\\ e^{-|t-(1/2)|}(16t^2-24t+18) & \text{if } t\ge\frac{3}{4}. \end{cases}$$

This function presents a discontinuity at $t=\frac{1}{4}$, a discontinuity in the first derivative at $t=\frac{1}{2}$, and a discontinuity in the second derivative at $t=\frac{3}{4}$. By visual inspection, it is possible to detect the discontinuities in the signal and also in the first derivative. However in the second derivative it is not possible (Fig. A1). Using, for instance, the first three decomposition levels, someone using the wavelet coefficients can detect all discontinuities. Thus, based on the amplitude of the wavelet coefficient, it is possible to quantify the kinds of disturbance levels that exist in the signal.

References

Abry, P., 1997. Ondelettes et turbulence. Multiresolutions, algorithmes de decomposition, invariance d'chelles. Diderot Editeur, Paris.

Badruddin, Y.P., 2002. Study of the e effectiveness of various solar wind parameters in the development of geomagnetic storms during interplanetary events. Turk. J. Phys., 391–402

Bothmer, V., Schwenn, R., 1994. Eruptive prominences as sources of magnetic clouds in the solar wind. Space Sci. Rev. 70, 215.

Bothmer, V., Rust, D.M., 1997. The field configuration of magnetic clouds and the solar cycle. Geophys. Monogr., 139–146, AGU

Bothmer, V., Schwenn, R., 1998. The structure and origin of magnetic clouds in the solar wind. Ann. Geophys. 16 (1), 1–24.

Burlaga, L.F., Sittler, E., Mariani, F., Schwenn, R., 1981. Magnetic loop behind an interplanetary shock: Voyager, Helios and IMP 8 observations. J. Geophys. Res. 86, 6673–6684.

Burlaga, L.F., Behannon, K.W., 1982. Magnetic clouds: voyager observations between 2 and 4 AU. Sol. Phys. 81 (1), 181–192.

Cane, H.V., Richardson, I.G., 2003. Interplanetary coronal mass ejections in the near-Earth solar wind during 1996–2002. J. Geophys. Res. 108 (A4), 1156.

Chian, A.C.-L., Muñoz, P.R., 2011. Detection of current sheets and magnetic reconnections at the turbulent leading edge of an interplanetary coronal mass ejection. Astrophys. J. Lett. 733 (2), L34.

Dasso, S., Mandrini, C.H., Démoulin, P., Luoni, M.L., Gulisano, A.M., 2005. Large scale MHD properties of interplanetary magnetic clouds. Adv. Space Res. 35 (5), 711–724.

Daubechies, I., 1990. The wavelet transform, time-frequency localization and signal analysis. IEEE Trans. Inf. Theory 36 (5), 961–1005.

Démoulin, P., Dasso, S., 2009. Causes and consequences of magnetic cloud expansion. Astron. Astrophys. 498 (2), 551–566.

Domingues, M.O., Gomes, S.M., Roussel, O., Schneider, K., 2008. An adaptive multiresolution scheme with local time stepping for evolutionary PDEs. J. Comput. Phys. 227 (8), 3758–3780.

Domingues, M.O., Gomes, S.M., Roussel, O., Schneider, K., 2009. Space-time adaptive multiresolution methods for hyperbolic conservation laws: applications to compressible Euler equations. Appl. Numer. Math. 59, 2303–2311.

Domingues, M.O., Gomes, S.M., Roussel, O., Schneider, K., 2011. Adaptive multiresolution methods. Eur. Ser. Appl. Ind. Math. Proc. 34, 1–96.

Dungey, J.W., 1961. Interplanetary magnetic field and the auroral zones. Phys. Rev. Lett. 6, 47–48.

Farrugia, C.J., Burlaga, L.F., Osherovich, V.A., Richarson, I.G., Freeman, M.P., Lepping, R.P., Lazarus, A., 1993. A study of an expanding interplanetary magnetic cloud and its interaction with the Earth's magnetosphere. J. Geophys. Res.: Space Phys. 98 (A5), 7621–7632.

Goldstein, H., 1983. On the field configuration in magnetic clouds. In: Neugebauer, M. (Ed.), Solar Wind Five, NASA Conference Publication, vol. 22 (22), pp. 731–733.

Gonzalez, W., Joselyn, J., Kamide, Y., Kroeshl, H.W., Rostoker, G., Tsurutani, B.T., Vasyliunas, V.M., 1994. What is a geomagnetic storm? J. Geophys. Res. 99, 5771–5792.

Gonzalez, W., Tsurutani, B.T., 1987. Criteria of interplanetary parameters causing intense magnetic storms ($dst < -100nt$). Planet. Space Sci. 35, 1101–1109.

Gosling, J.T., 1990. Coronal mass ejections and magnetic flux ropes in interplanetary space, in physics of magnetic flux ropes. In: Russel, C.T., Priest, E.R., Lee, L.C. (Eds.), Geophysical Monograph Series, vol. 58. AGU, pp. 3518–3528.

Hubbard, B.B., 1990. The World According to Wavelets: the Story of a Mathematical Technique in the making. Ak Peters Series. A.K. Peters, Wellesley, Massachusetts, USA.

Huttunen, K.E.J., Bothmer, V., Koskinen, H.E.J., 2005. Properties and geoeffectiveness of magnetic clouds in the rising, maximum and early declining phases of solar cycle 23. Ann. Geophys. 23, 1–17.

Iyemori, T., 1990. Storm-time magnetospheric currents inferred from mid-latitude geomagnetic field variations. J. Geomagn. Geoelectr. 42 (11), 1249–1265.

Klein, L.W., Burlaga, L.F., 1982. Interplanetary magnetic clouds at 1 AU. J. Geophys. Res. 87, 613–624.

Lepping, R.P., Burlaga, L.F., Jones, J.A., 1990. Magnetic field structure of interplanetary magnetic clouds at 1 AU. J. Geophys. Res. 951, 11957–11965.

Lepping, R.P., Berdichevsky, D., 2000. Interplanetary magnetic clouds, sources, properties, modelling, and geomagnetic relationship. Recent Res. Dev. Geophys. 3, 77–96.

Lynch, B., Zurbuchen, T., Fisk, L., Antiochos, S., 2003. Internal structure of magnetic clouds: plasma and composition. J. Geophys. Res. 108 (A6), 1239–1253.

Mallat, S., 1997. A Wavelet Tour of Signal Processing. AP Professional, London. (https://www.ceremade.dauphine.fr/~peyre/wavelet-tour/).

Mendes, O., Domingues, M.O., Mendes da Costa, A., 2005. Wavelet analysis applied to magnetograms. J. Atmos. Sol.-Terr. Phys. 67, 1827–1836.

Mendes da Costa, A., Domingues, M.O., Mendes, O., Brum, C.G.M., 2011. Interplanetary medium condition effects in the south atlantic magnetic anomaly: a case study. J. Atmos. Sol.-Terr. Phys. 73 (11–12), 1478–1491.

Müller, S., 2003. Adaptive multiscale schemes for conservation laws. In: Lectures Notes in Computational Science and Engineering, vol. 27, Heidelberg Springer.

Mulligan, T., Russel, C.T., Luhmann, J., 1998. Solar cycle evolution of the structure of magnetic clouds in the inner Heliosphere. Geophys. Res. Lett. 25 (15), 2959–2962.

Nieves-Chinchilla, T., Hidalgo, M., Sequeiros, J., 2005. Magnetic clouds observed at 1 AU during the period 2000–2003. Sol. Phys. 232, 105–126.

Ojeda, G., Calzadilla, A., Lazo, B., Alazo, K., Savio, S., 2005. Analysis of behavior of solar wind parameters under different IMF conditions using two nonlinear dynamics techniques. J. Atmos. Sol.-Terr. Phys. 67, 1859–1864.

Ojeda, G., Mendes, A.O., Calzadilla, M.A, Domingues, M.O., 2013. Spatio-temporal entropy analysis of the magnetic field to help magnetic cloud characterization. J. Geophys. Res. 118, 5403–5414. doi: http://dx.doi.org/10.1002/jgra.50504.

Owens, M.J., Cargill, P.J., Pagel, C., Siscoe, G.L., Crooker, N.U., 2005. Characteristic magnetic field and speed properties of interplanetary coronal mass ejections and their sheath regions. J. Geophys. Res. 110 (A01105), 1–9.

Richardson, I.G., Cane, H.V., 2010. Near-Earth interplanetary coronal mass ejections during solar cycle 23 (1996–2009): catalog and summary of properties. Sol. Phys. 264 (1), 189–237.

SPIDR, 2008. ⟨http://spidr.ngdc.noaa.gov/spidr/index.jsp⟩.

Sugiura, M., Kamei, T., 1986. Equatorial Dst index 1957–1986. In: Berthelier, A., Menvielle, M. (Eds.), IAGA Bulletin, vol. 40. S GI Publ. Off., Saint. Maur-des-Fosses, France.

Wanliss, J.A., Showalter, K.M., 2006. High-resolution global storm index: Dst versus SYM-H. J. Geophys. Res.: Space Phys. (1978–2012) 111 (A2).

Wu, C.C., Lepping, R.P., Gopalswamy, N., 2003. Variations of magnetic clouds and CMEs with solar activity cycle. In: Proceedings of the ISCS 2003 Symposium, "Solar variability as an input to the Earth's Enviroment", Slovakia, ESA, vol. 1, pp. 429–432.

Wu, C.C., Liou, K., Lepping, R.P., Meng, C.I., 2004. Identification of substorms within storms. J. Atmos. Sol.-Terr. Phys. 66 (2), 125–132.